Deep-Sea Research II 138 (2017) 63–73

Contents lists available at ScienceDirect

Deep-Sea Research II

journal homepage: www.elsevier.com/locate/dsr2

Controls of primary production in two phytoplankton blooms in the Antarctic Circumpolar Current

C.J.M. Hoppe [a,*], C. Klaas [a], S. Ossebaar [b], M.A. Soppa [a], W. Cheah [a,c], L.M. Laglera [d], J. Santos-Echeandia [e], B. Rost [a], D.A. Wolf-Gladrow [a], A. Bracher [a,f], M. Hoppema [a], V. Strass [a], S. Trimborn [a,g]

[a] Alfred Wegener Institute-Helmholtz Centre for Polar and Marine Research, Am Handelshafen 12, 27570 Bremerhaven, Germany
[b] NIOZ-Royal Netherlands Institute for Sea Research, Landsdiep 4, 1797 SZ't Horntje, Texel, The Netherlands
[c] Research Center for Environmental Changes, Academia Sinica, 128 Academia Road, 11529 Taipei, Taiwan
[d] FITRACE, Departamento de Química, Universidad de las Islas Baleares, Cra. de Valldemossa, Palma, Balearic Islands, 07122, Spain
[e] Marine Biogeochemistry, Instituto de Investigaciones marinas (CSIC), Eduardo Cabello 6, 36208 Vigo, Spain
[f] Institute of Environmental Physics, University Bremen, Otto Hahn Allee 1, 28359 Bremen, Germany
[g] Marine Botany, University Bremen, Leobener Straße NW2, 28359 Bremen, Germany

ARTICLE INFO

Available online 3 November 2015

Keywords:
Biological pump
Nutrient budgets
Primary productivity
Southern Ocean

ABSTRACT

The Antarctic Circumpolar Current has a high potential for primary production and carbon sequestration through the biological pump. In the current study, two large-scale blooms observed in 2012 during a cruise with R.V. Polarstern were investigated with respect to phytoplankton standing stocks, primary productivity and nutrient budgets. While net primary productivity was similar in both blooms, chlorophyll *a* –specific photosynthesis was more efficient in the bloom closer to the island of South Georgia (39 °W, 50 °S) compared to the open ocean bloom further east (12 °W, 51 °S). We did not find evidence for light being the driver of bloom dynamics as chlorophyll standing stocks up to 165 mg m^{-2} developed despite mixed layers as deep as 90 m. Since the two bloom regions differ in their distance to shelf areas, potential sources of iron vary. Nutrient (nitrate, phosphate, silicate) deficits were similar in both areas despite different bloom ages, but their ratios indicated more pronounced iron limitation at 12 °W compared to 39 °W. While primarily the supply of iron and not the availability of light seemed to control onset and duration of the blooms, higher grazing pressure could have exerted a stronger control toward the declining phase of the blooms.

1. Introduction

Oceanic phytoplankton account for about half of the global primary production, thereby providing the basis of marine food webs and exerting a major control on biogeochemical cycles and global climate (Falkowski et al., 1998; Field et al., 1998). The supply of nutrients such as nitrate, phosphate and silicate to the photic zone (i.e. 'new' nutrients) constrains the biologically-mediated export of organic carbon to the deep ocean (Dugdale and Goering, 1967; Eppley and Peterson, 1979; Longhurst and Harrison, 1989). The strength of this biological carbon pump can be estimated from the degree to which these nutrients are consumed as well as the carbon to nutrient ratios in the organic matter sinking to depth.

One area with great potential for an increase in both new and recycled production is the Antarctic Circumpolar Current (ACC). As concentrations of nitrate and phosphate are high, primary production is limited by other controlling factors (Priddle et al., 1992; Moore et al., 2000). More specifically, productivity in the ACC region is thought to be controlled by interactions between light availability (Mitchell and Holm-Hansen, 1991; Nelson and Smith, 1991), iron supply (Martin, 1990; de Baar et al., 1995), silicate limitation (Brzezinski et al., 2003), and the effect of grazing (Dubischar and Bathmann, 1997; Atkinson et al., 2001). More recent studies suggest that iron is the primary limiting factor in these open ocean areas (Smetacek et al., 2012). Phytoplankton blooms in the ACC tend to occur downstream of land masses and have been associated with fronts, islands and bathymetric features, which increase the input of iron and other trace metals into the surface waters (Moore et al., 1999; Blain et al., 2001; Borrione and Schlitzer, 2013). In the Atlantic sector of the ACC, high phytoplankton standings stocks and production rates have been observed in the

* Corresponding author. Tel.: +49 471 4831 2096.
E-mail address: Clara.Hoppe@awi.de.(C.J.M. Hoppe)

http://dx.doi.org/10.1016/j.dsr2.2015.10.005

Antarctic Polar Frontal Zone (APFZ; Bathmann et al., 1997; Bracher et al., 1999; Moore and Abbott, 2000; Tremblay et al., 2002). In this particular region, an alleviation of light limitation through upper water column stratification in spring was proposed as a trigger for the development of phytoplankton blooms. Finally, the termination of blooms is often caused by a combination of grazing pressure as well as iron and silicate limitation (Abbott et al., 2000; Tremblay et al., 2002).

Attempts to disentangle the effects of potential factors controlling bloom dynamics are complicated by the fact that these different factors tend to co-vary and also interact with each other (e.g. iron limitation decreases photoadaptive capabilities, thereby affecting light limitation; Sunda and Huntsman, 1997; Petrou et al., 2014). The aim of the present study was, therefore, to understand how different environmental factors influence the biomass, primary productivity, nutrient usage and the potential for carbon sequestration in two large-scale phytoplankton blooms with a putatively different iron supply.

2. Material and methods

2.1. Cruise track and sampling locations

Sampling was conducted in the framework of the 'Eddy-Pump' project during the ANT-XXVIII/3 expedition on-board the German research vessel Polarstern (Wolf-Gladrow, 2013) between January and March 2012 in two survey areas. In addition to physical properties, nutrient and chlorophyll concentrations as well as primary productivity were determined at 10 stations in a land-remote bloom at 50–52 °S and 13.5–11.5 °W (hereafter 12 °W bloom) and at 9 stations in a bloom downstream of South Georgia at 48–52 °S and 37–39 °W (hereafter 39 °W bloom; Fig. 1). Water samples for all measured parameters except iron (see below), were obtained at discrete depths (10, 20, 40, 60, 80 and 100 m) from Niskin bottles attached to a Conductivity Temperature Depth (CTD) rosette. The mixed layer depth (MLD) was defined as a change of density of 0.02 kg m^{-3} relative to the uppermost value of each CTD vertical profile (Cisewski et al., 2005, Strass et al., 2017). It should be noted that at station PS79/085 (the out-station in the 12 °W area), chlorophyll biomass was evenly distributed to a deeper pycnocline at a depth of 82 m even though the MLD determined was 30 m only.

2.2. Macronutrient measurements and nutrient deficit calculations

Macronutrients were measured colorimetrically using a Technicon TRAACS 800 auto-analyzer (Seal Analytical) on board the ship. Orthophosphate (PO_4^{3-}) was measured at 880 nm after the formation of molybdophosphate-complexes (Murphy and Riley, 1962).

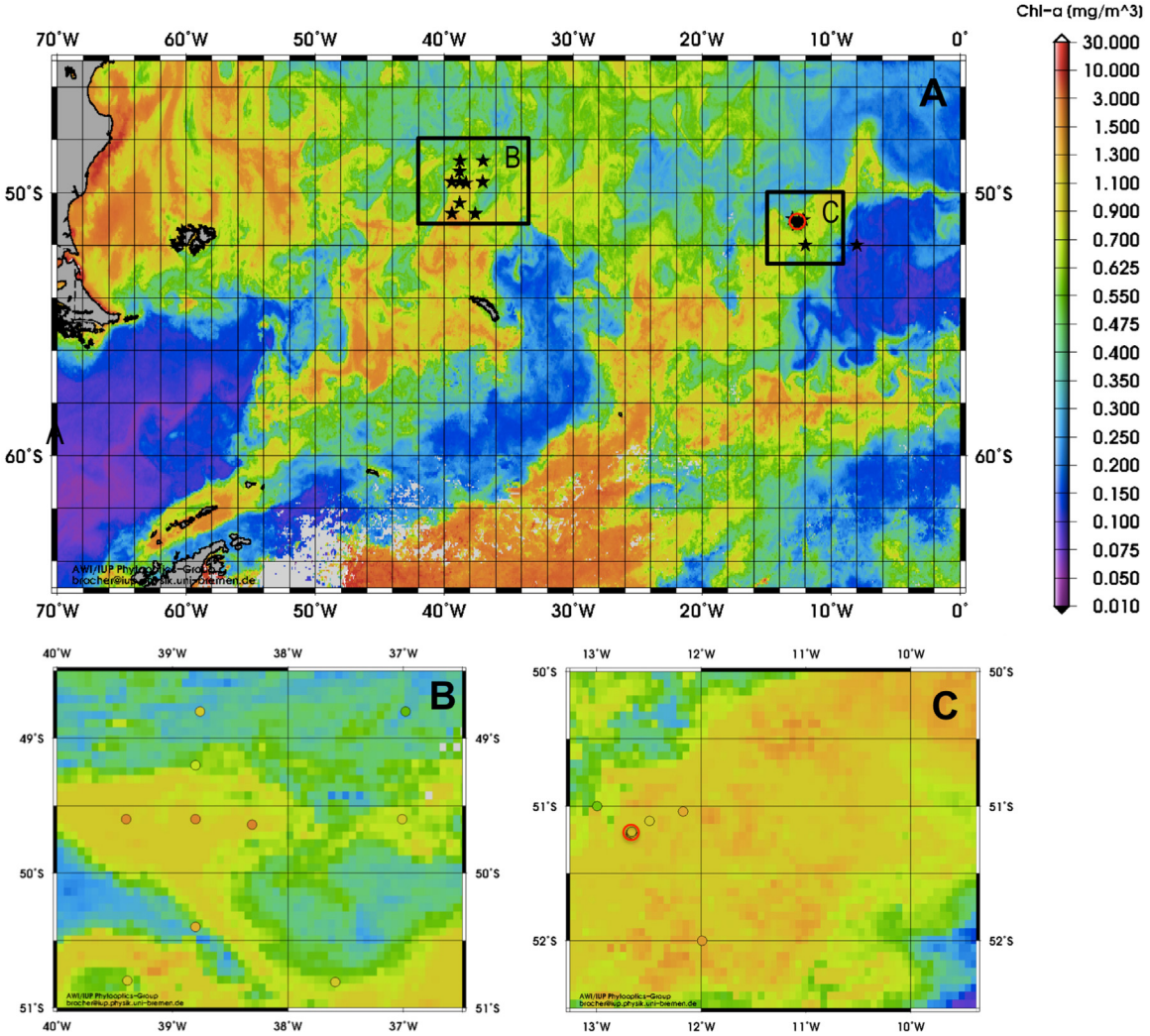

Fig. 1. Satellite-based Chl *a* maps – Mean Chl *a* concentrations (mg m^{-3}) during February 2012 derived from the satellite MERIS Polymer product. Stars indicate sampling locations during the ANT-XXVIII/3 cruise. Detailed view on the 39 °W bloom north of South Georgia (B) and the 12 °W bloom (C) with circles indicating station positions where Chl *a* concentrations were measured in-situ; red circle indicates the time-series station.

Orthosilicate ($Si(OH)_4$) was measured at 820 nm after formation of silica-molybdenum complexes with oxalic acid being added to prevent the formation of phosphate-molybdenum (Strickland and Parsons, 1968). After nitrate reduction through a copperized cadmium coil, nitrate plus nitrite ($NO_3^- + NO_2^-$) was measured at 550 nm after complexation with sulphanylamide and naphtylethylenediamine (Grasshoff et al., 1999). Complex formation without the reduction step was used to determine nitrite concentrations. Nitrate is calculated by subtracting the nitrite value from the '$NO_3- + NO_2-$' value (Grasshoff et al., 1999).

Prior to analysis, all samples and standards were brought to 22 °C in about 2 h. Concentrations were recorded in mmol m^{-3} at this temperature. Calibration standards were diluted from stock solutions of the different nutrients in 0.2 µm filtered low nutrient seawater. During every run, a freshly diluted mixed nutrient standard, containing silicate, phosphate and nitrate, the so-called 'NIOZ nutrient cocktail', was measured in triplicate. Every 2 weeks, a sterilised 'Reference Material Nutrient Sample' (JRMNS, Kanso Technos, Japan) containing known concentrations of silicate, phosphate, nitrate and nitrite in Pacific Ocean water was analysed in triplicate. The cocktail and the JRMNS were both used to monitor the performance of the analyser. Finally, the NIOZ nutrient cocktail was used to adjust all data by multiplying with the offset factor derived from the differences between assigned and measured nutrient concentrations. The average standard deviations of the NIOZ nutrient cocktail measurements were 0.02 mmol m^{-3} for phosphate, 0.59 mmol m^{-3} for silicate and 0.13 mmol m^{-3} for nitrate ($n=113$).

Surface nutrient concentrations were calculated as the weighted average of the measured values for sampling depths 10–60 m, accounting for differences in sampling frequency with increasing depth. Nutrient deficits were calculated at each station as the differences between the nutrient concentration in remnant Antarctic Winter Water (AWW) in the layer below the seasonal pycnocline and the average concentrations above that (Jennings et al., 1984; Hoppema et al., 2000). The nutrient deficit per m^3 at each station was averaged over the different depths, while the deficit per m^2 was calculated by integrating the deficits from 10 to 120 m data for the water column of 0–120 m. It should be noted that nutrient deficits are suitable estimates for annual net community production only if vertical and lateral mixing in both the temperature minimum and the surface layer are small (Jennings et al., 1984; Hoppema et al., 2000; Hoppema et al., 2007). The deficits thus represent a somewhat larger area than just the station location. The AWW layer, which was characterised by a well-defined potential temperature minimum (Z_{tmin}) in the CTD profiles, was situated at 150 ± 15 m water depth during this cruise. AWW nutrient concentrations were similar in both bloom areas (2.1 ± 0.1 mmol m^{-3} for phosphate, 30.1 ± 6.1 mmol m^{-3} for silicate and 30.6 ± 1.4 mmol m^{-3} for nitrate; $n=113$; Fig. 2). Deficit ratios (i.e. $Si(OH)_4$:NO_3 and NO_3:PO_4) were calculated after averaging the nutrient deficits from the different depths at each station.

2.3. Iron sampling and measurements

Samples for total dissolved iron (TDFe) measurements were collected from the upper 300 m of the water column in metal free GOFLO bottles attached to a Kevlar line. Samples were immediately online filtered through trace-metal clean 0.22 µm sterile capsules (Sartobran 300, Sartorius) and subsequently collected in low-density polyethylene bottles. TDFe was determined on-board by voltammetry following the protocol described by Laglera et al. (2013).

2.4. Irradiance estimates

Solar irradiance was measured continuously at one-minute intervals using a RAMSES hyperspectral radiometer (TriOS GmbH, Germany) placed on the uppermost deck of the ship to avoid shading. The sensor measured downwelling incident

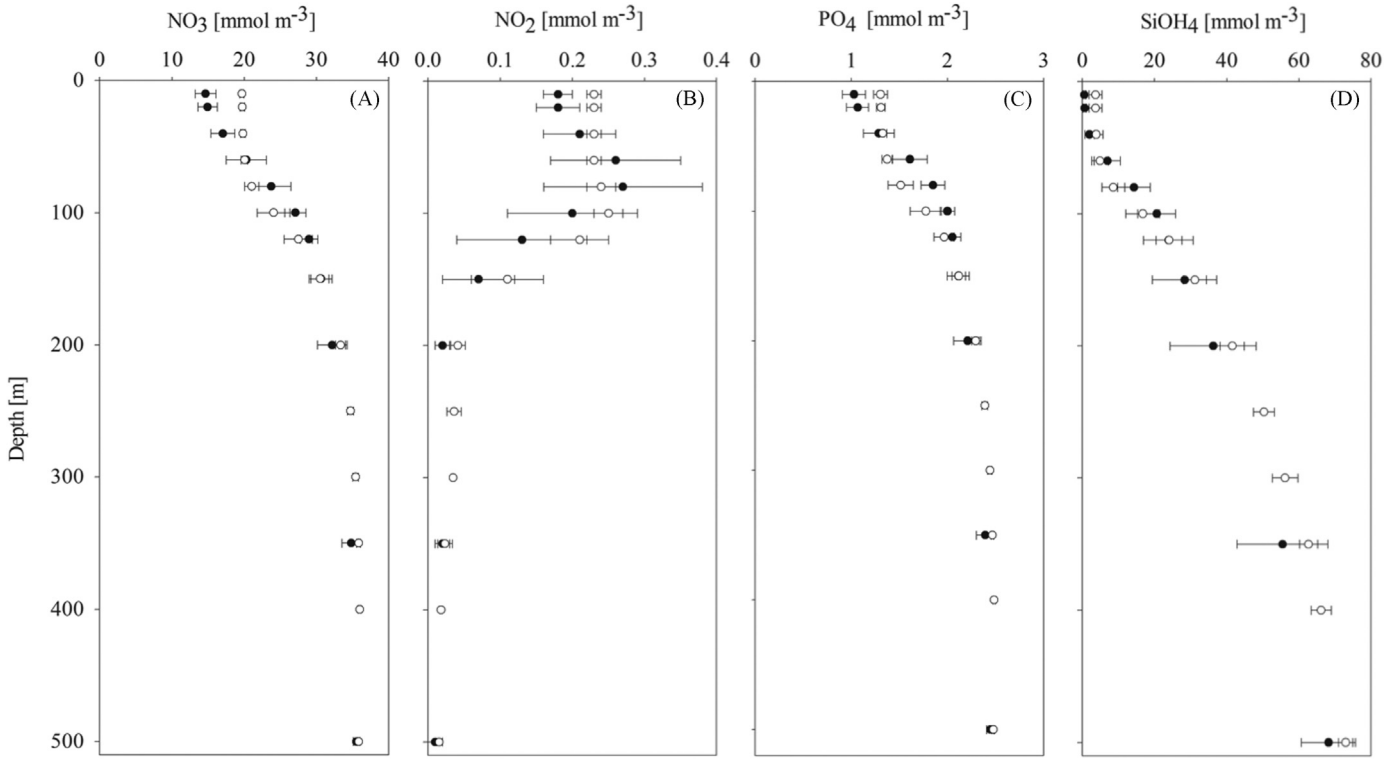

Fig. 2. Average nutrient profiles – Concentrations of nitrate (A), nitrite (B), phosphate (C) and silicate (D) in the top 500 m from the 12 °W bloom (open symbols) and the 39 °W bloom north of South Georgia (filled symbols).

sunlight from 350 to 950 nm with a spectral resolution of 3.3 nm. Plane photosynthetically active radiation (PAR) was calculated as the integral of irradiances from 400 to 700 nm. Daily PAR values [mol photons $m^{-2}\,d^{-1}$] were then calculated by integrating the PAR values from the start to the end of each incubation (~24 h).

2.5. Chlorophyll a

Chlorophyll *a* (Chl *a*) concentrations were determined by two methods: fluorometry (Chl a_{FLUO}) and high performance liquid chromatography (HPLC; Chl a_{HPLC}). Except for stations PS79/160 and PS79/175, where Chl a_{FLUO} data were used, Chl *a* estimates are based on Chl a_{HPLC} data. The two Chl *a* datasets produced similar results, showing a significant correlation and only minimal differences ($r^2=0.97$, $p<0.001$, $n=104$, Chl $a_{FLUO}=0.990*$ Chl $a_{HPLC}+0.0837$).

For the Chl a_{FLUO} determination, samples were filtered onto 25 mm diameter GF/F filters (Whatman; 0.7 μm nominal pore size) at a vacuum of < 100 mmHg. Filters were immediately transferred into centrifuge tubes containing 10 mL of 90% acetone and 1 cm^3 of glass beads. The tubes were sealed and stored at −20 °C for at least 30 min and up to 24 h. Chl a_{FLUO} was extracted by placing the centrifuge tubes in a grinder for 3 min followed by centrifugation at 0 °C. The supernatant was poured into quartz tubes and the Chl a_{FLUO} content was quantified in a 10-AU fluorometer (Turner). Calibration of the fluorometer was carried out at the beginning and at the end of the cruise, diverging by 2%. Chl a_{FLUO} content was calculated using the equation given in Knap et al. (1996) and the average parameter values from the two calibrations.

For the Chl a_{HPLC} determinations, samples were filtered onto 25 mm diameter GF/F filters (Whatman) at a vacuum of < 100 mmHg. Filters were shock-frozen in liquid nitrogen and stored at −80 °C until analysis in the home laboratory following the method described by Hoffmann et al. (2006) as detailed in Cheah et al. (2017). For calculating Chl a_{HPLC} the sum of concentrations of monovinyl-, divinylchlorophyll *a* and chlorophyllide *a* was taken (divinyl chlorophyll *a* was not detected in our samples).

Vertical plankton net samples were used to qualitatively determine the dominant phytoplankton functional types by means of light microscopy.

2.6. Particulate organic carbon and nitrogen

Samples for particulate organic carbon (POC) and nitrogen (PON) were filtered onto pre-combusted (15 h, 500 °C) glass fibre filters (GF/F, Whatman). Filters were stored at −20 °C and processed according to Lorrain et al. (2003). Analyses were performed using a CHNS-O elemental analyser (Euro EA 3000, HEKAtech).

2.7. Primary productivity

Net primary production rates (NPP) were determined in duplicates by the incubation of 20 mL seawater sample spiked with 20 μCi $NaH^{14}CO_3$ (53.1 mCi $mmol^{-1}$; Perkin Elmer) in a 20 mL glass scintillation vial for 24 h in a seawater cooled on-deck incubator. Seawater samples from 6 depths (10, 20, 40, 60, 80 and 100 m) were incubated at different irradiances, which were achieved with neutral density filters decreasing incoming light to 25%, 12.5%, 6.3%, 3.1%, 1.6% and 0.8% of downwelling PAR above the ocean surface.

After the addition of the $NaH^{14}CO_3$ spike, 0.1 mL aliquots were immediately removed and mixed with 10 mL of scintillation cocktail (Ultima Gold AB, PerkinElmer). After 2 h, these samples were counted with a liquid scintillation counter (Tri-Carb 2900TR, PerkinElmer) to determine the total amount of added $NaH^{14}CO_3$ (100%). For blank determination, one additional replicate per sample was immediately acidified with 0.5 ml 6 N HCl. After the outdoor incubation of the samples over 24 h, ^{14}C incorporation was stopped by adding 0.5 mL 6 N HCl to each vial. The vials were then left to degas overnight, thereafter 15 ml of scintillation cocktail (Ultima Gold AB) were added and samples were measured after 2 h with the same liquid scintillation counter. NPP rates [mg C $m^{-3}\,d^{-1}$] at each sample depth were calculated as follows:

$$\mathrm{NPP}\left[\mathrm{mg\,C\,m^{-3}\,d^{-1}}\right] = (\mathrm{DIC} * (\mathrm{DPM_{sample}} - \mathrm{DPM_{blank}}) * 1.05) / (\mathrm{DPM_{100\%}} * t) \quad (1)$$

where DIC is the concentration of dissolved inorganic carbon [μmol kg^{-1}], t is the incubation time [h] and 1.05 is the factor describing the discrimination between incorporation of ^{14}C and ^{12}C. DPM_{blank}, DPM_{sample} and $DPM_{100\%}$ are the disintegration per minute measured by the scintillation counter for the blank, the sample and the determination of the total amount of added $NaH^{14}CO_3$, respectively. Chl *a*-specific carbon fixation ($NPP_{Chl\ a}$ [mg C [mg Chl *a*]$^{-1}$ d^{-1}]) was calculated by dividing the depth-specific NPP value by the depth-specific Chl *a* concentrations. Column-integrated $NPP_{Chl\ a}$ and primary productivity (NPP [mg C $m^{-2}\,d^{-1}$]) were derived by integrating values for 100 m depth.

2.8. Satellite Chl a maps

Weekly satellite maps of Chl *a* were used to study the development of the blooms. The comparison of satellite derived Chl *a* concentrations with the in-situ values measured at the two bloom locations was based on daily maps. The Chl *a* maps were derived using the POLYMER level-3 product of the Medium Resolution Imaging Spectrometer (MERIS) at a 0.02° spatial resolution (Steinmetz et al. 2011). POLYMER is an improved atmospheric correction algorithm for pixels contaminated by sun glint, thin clouds or heavy aerosol plumes. MERIS Polymer products improve the spatial coverage by almost a factor of two and have been proven successful for retrieving MERIS Ocean Colour products (Müller et al. 2015). The Chl *a* concentrations are retrieved using the standard OC4Me algorithm (Morel et al. 2007).

3. Results

3.1. Temporal and spatial development of the blooms

During austral summer (January–March) 2012, two large-scale phytoplankton blooms were observed in the APFZ (Fig. 1A). A comparison of all surface Chl *a* concentrations (< 10 m) derived by HPLC measurements with daily MERIS Polymer Chl *a* within the respective satellite pixel (Fig. 1B and C) revealed a reasonable correlation coefficient ($r^2=0.67$), low bias (0.17 mg m^{-3}) and low percentage error (33%) between the two approaches. Estimates of Chl *a* standing stocks from in-situ measurements and satellite-based products are thus in good agreement, showing a nearly perfect match for the bloom situated at 12 °W (Fig. 1C). A reasonable agreement was observed for the 39 °W bloom north of South Georgia, where satellite data tended to underestimate Chl *a* concentrations, particularly in the higher range of the measured values (Fig. 1B). Both blooms were dominated by diatoms (Klaas, unpubl. results; also indicated by silicate depletion in the surface waters, Fig. 2).

In the 12 °W bloom area (Fig. 1A and C), satellite Chl *a* maps indicated that a bloom developed from mid-December 2011 onwards and peaked in the first two weeks of January 2012 with Chl *a* concentrations of around 3 mg m^{-3}. Our in-situ sampling took place between January 26th and February 15th, i.e. in the declining phase of the bloom. Within these three weeks, a central

station (at 12 °6′W, 51 °2′S) was re-visited six times to investigate the temporal development of the bloom. The satellite data indicated that Chl *a* concentrations in the area quickly decreased within 5 days after the last sampling date to values lower than 1 mg m^{-3}.

The phytoplankton bloom at 39 °W (Fig. 1A and B) was located in the Georgia Basin, north of the island of South Georgia. Satellite Chl *a* maps indicated that the 39 °W bloom had already developed during mid-October and peaked in mid-December with surface Chl *a* concentrations reaching values higher than 3 mg m^{-3}. In-situ sampling took place between February 16th and March 3rd, in the declining phase of the bloom. Satellite data indicated that Chl *a* concentrations above 0.5 mg m^{-3} persisted at least until mid-March.

3.2. Phytoplankton standing stocks and primary productivity

In the 12 °W area, average MLD was 71 ± 14 m. The depth-integrated Chl *a* concentrations in the bloom ranged from 50 to 180 mg Chl *a* m^{-2} (Table 1) and were on average 120 ± 41 mg Chl *a* m^{-2}. Values were as low as 9 mg m^{-2} outside the bloom area (Table 2). NPP ranged from 800 to 2820 mg C m^{-2} d^{-1} (Table 1) and was on average 1750 ± 750 mg C m^{-2} d^{-1} (Table 2) in the bloom, and thus significantly higher than values outside the bloom area (160 mg C m^{-2} d^{-1}). Chl *a*-specific carbon fixation $NPP_{Chl\ a}$, a measure of photosynthetic efficiency, varied between 10.1 and 17.3 mg C [mg Chl *a*]$^{-1}$ d^{-1} (on average 14.4 ± 2.6 mg C [mg Chl *a*]$^{-1}$ d^{-1}) in the 12 °W bloom (Tables 1 and 2). The average depth-integrated molar POC:PON ratios in this area were 6.3 ± 0.6 (Table 2). Average daily PAR during primary production measurements in the 12 °W bloom was 12.3 ± 5.1 mol photons m^{-2} d^{-1} (Table 2).

In the 39 °W bloom north of South Georgia, average MLD was 35 ± 13 m. In-situ Chl *a* standing stocks ranged from 25 to 130 mg Chl *a* m^{-2} (Table 1), with an average of 60 ± 30 mg Chl *a* m^{-2} (Table 2). NPP (Table 1) in this region varied between 570 and 3020 mg C m^{-2} d^{-1} (on average 1370 ± 830 mg C m^{-2} d^{-1}). $NPP_{Chl\ a}$ varied between 14.4 and 30.3 mg C [mg Chl *a*]$^{-1}$ d^{-1} (average of 19.4 ± 5.5 mg C [mg Chl *a*]$^{-1}$ d^{-1}). In the 39 °W bloom, average depth-integrated molar POC:PON ratios (Table 2) were 5.9 ± 0.5. Average daily PAR during primary production measurements in this bloom was 15.7 ± 6.1 mol photons m^{-2} d^{-1} (Table 2).

Light profiles in the surface ocean were measured at 6 stations in the 12 °W bloom area (with an average depth of the euphotic zone, Z_{eu} [0.8%], of 29.6 ± 7.6 m) and only one station in the 39 °W bloom area (Z_{eu} [0.8%]=21.5 m), indicating similar euphotic depths in both blooms.

3.3. Nutrient concentrations and deficits

In the 12 °W bloom area, average surface nutrient concentrations (10 m depth) were 19.7 ± 0.3 mmol NO_3 m^{-3}, 1.3 ± 0.1 mmol PO_4 m^{-3}, and 4.1 ± 3.1 mmol $Si(OH)_4$ m^{-3} (Fig. 2). The average nutrient concentrations in the euphotic zone (10–60 m) were 20.6 ± 0.5 mmol NO_3 m^{-3}, 1.4 ± 0.1 mmol PO_4 m^{-3}, and 6.6 ± 2.7 mmol $Si(OH)_4$ m^{-3} (Table 2). Average integrated nutrient deficits in this area were 1090 ± 110 mmol NO_3 m^{-2}, 75 ± 7 mmol PO_4 m^{-2}, and 2710 ± 300 mmol $Si(OH)_4$ m^{-2} (Table 2) with a $Si(OH)_4$:NO_3 deficit ratio of 2.5 ± 0.3 mol mol^{-1} and a NO_3:PO_4 deficit ratio of 14 ± 1 mol mol^{-1} (Table 2, Fig. 3). Average total dissolved iron (TDFe) concentrations in the upper 100 m of the water column were 0.12 ± 0.03 nM (Table 2, Fig. 4).

In the 39 °W bloom area, average surface nutrient concentrations (10 m depth) were 14.9 ± 1.8 mmol NO_3 m^{-3}, 1.0 ± 0.1 mmol PO_4 m^{-3}, and 0.6 ± 0.5 mmol $Si(OH)_4$ m^{-3} (Fig. 2). Average nutrient concentrations of the euphotic zone (10–60 m) were 16.3 ± 1.8 mmol NO_3 m^{-3}, 1.2 ± 0.1 mmol PO_4 m^{-3} and 2.2 ± 1.3 mmol $Si(OH)_4$ m^{-3} (Table 2). Resulting average integrated surface nutrient deficits in the

Table 1
100 m Depth-integrated Chl *a* standing stocks [mg m^{-2}], primary productivity NPP [mg C m^{-2} d^{-1}], photosynthetic efficiency $NPP_{Chl\ a}$ [mg C (mg Chl *a*)$^{-1}$ d^{-1}], total PAR during on-deck incubations [mol photons m^{-2} d^{-1}]. Star symbol denotes central station in 12 °W bloom.

Bloom area	Station #	Date	Longitude [°W]	Latitude [°S]	MLD [m]	Chl *a* [mg m^{-2}]	PAR [mol photons m^{-2} d^{-1}]	NPP [mg C m^{-2} d^{-1}]	$NPP_{Chl\ a}$ [mg C (mg Chl *a*)$^{-1}$ d^{-1}]
Outstation 12 °W	PS79/085-03	26.01.12	8.00	52.00	30	9	14.45	161	17.6
	PS79/086-02	29.01.12	11.99	52.00	87	180	11.27	2587	14.4
	PS79/091-05*	03.02.12	12.67	51.21	56	166	16.40	2816	17.0
	PS79/114-01*	08.02.12	12.67	51.20	78	143	18.75	2447	17.1
	PS79/128-10*	12.02.12	12.65	51.21	89	117	13.80	1669	14.2
	PS79/136-08*	14.02.12	12.66	51.20	55	85	17.03	1050	12.3
	PS79/137-07	15.02.12	12.17	51.04	84	136	8.68	1380	10.1
	PS79/138-02	15.02.12	12.49	51.11	65	88	5.65	1020	11.5
	PS79/139-03	15.02.12	12.99	51.00	57	52	6.01	796	15.4
	PS79/140-12*	17.02.12	12.66	51.19	68	115	19.31	1998	17.3
39 °W	PS79/147-01	25.02.12	37.01	49.60	28	54	15.58	n.d.	n.d.
	PS79/149-01	25.02.12	36.98	48.80	12	25	13.17	573	22.7
	PS79/155-01	26.02.12	37.59	50.81	23	60.	5.28	769	12.8
	PS79/160-01	27.02.12	38.80	50.40	42	n.d.	5.27	640	n.d.
	PS79/165-05	28.02.12	39.40	49.60	40	89	17.29	1644	18.4
	PS79/168-01	29.02.12	38.76	48.80	43	73	20.29	1052	14.4
	PS79/169-01	29.02.12	38.80	49.20	44	39	19.06	786	20.3
	PS79/170-01	29.02.12	38.80	49.60	53	129	19.61	2220	16.1
	PS79/174-09	01.03.12	38.31	49.64	39	100	17.76	3023	30.3
	PS79/175-01	03.03.12	39.39	50.80	30	79	19.49	1575	20.0

Table 2
Comparison of phytoplankton biomass, productivity and POC:PON ratios as well as average 10–60 m nutrient concentrations, nutrient deficits and average deficit concentrations as well as deficit ratios and 100 m depth-averaged TDFe concentrations for the two bloom areas investigated. Values denote average (± 1s.d.).

Parameter	12 °W bloom area			39 °W bloom		
Chl *a* [mg Chl *a* m^{-2}]	120	± 41	(n=9)	63	± 29	(n=9)
Net Primary Productivity [mg C m^{-2} d^{-1}]	1751	± 747	(n=9)	1365	± 832	(n=10)
$NPP_{Chl\ a}$ [mg C (mg Chl *a*)$^{-1}$ d^{-1}]	14	± 3	(n=9)	19	± 5	(n=8)
POC:PON [mol mol^{-1}]	6.3	± 0.6	(n=25)	5.9	± 0.5	(n=24)
POC:Chl *a* [g:g]	0.03	± 0.01	(n=8)	0.04	± 0.02	(n=5)
PAR [mol photons m^{-2} d^{-1}]	13	± 5	(n=9)	15	± 6	(n=9)
MLD [m]	71	± 14	(n=10)	35	± 13	(n=10)
NO_3 [mmol m^{-3}]	19.9	± 0.5	(n=35)	16.3	± 1.8	(n=26)
PO_4 [mmol m^{-3}]	1.3	± 0.1	(n=35)	1.2	± 0.1	(n=26)
$Si(OH)_4$ [mmol m^{-3}]	4.5	± 3.1	(n=35)	2.2	± 1.3	(n=26)
NO_3 deficit concentration [mmol m^{-3}]	9.1	± 0.9	(n=35)	10.2	± 2.6	(n=26)
PO_4 deficit concentration [mmol m^{-3}]	0.6	± 0.1	(n=35)	0.6	± 0.2	(n=26)
$Si(OH)_4$ deficit concentration [mmol m^{-3}]	22.6	± 2.5	(n=35)	19.7	± 5.3	(n=26)
NO_3 deficit [mmol m^{-2}]	1087	± 108	(n=35)	1219	± 307	(n=26)
PO_4 deficit [mmol m^{-2}]	75	± 7	(n=35)	68	± 18	(n=26)
$Si(OH)_4$ deficit [mmol m^{-2}]	2712	± 303	(n=35)	2359	± 631	(n=26)
NO_3:PO_4 deficit [mol mol^{-1}]	14.4	± 0.9	(n=35)	17.9	± 0.9	(n=26)
$Si(OH)_4$:NO_3 deficit [mol mol^{-1}]	2.5	± 0.3	(n=35)	2.0	± 0.4	(n=26)
TDFe [nM]	0.12	± 0.03	(n=48)	0.14	± 0.03	(n=11)

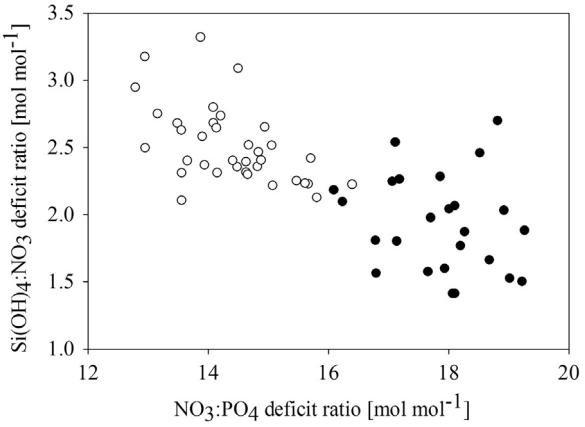

Fig. 3. Nutrient deficit ratios. Deficit ratios for $Si(OH)_4$:NO_3 versus NO_3:PO_4 [mol mol^{-1}] for all stations in the 12 °W bloom (open symbols) and the 39 °W bloom (filled symbols).

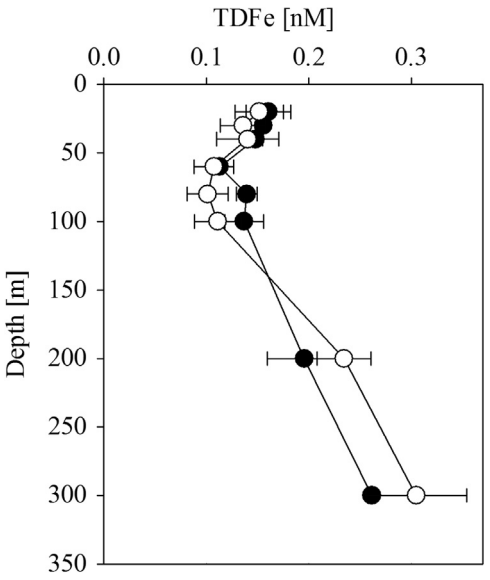

Fig. 4. Average total dissolved iron (TDFe) profiles for all stations sampled in the 12 °W bloom (n=8; open symbols) and the 39 °W bloom (n=2; filled symbols).

39 °W bloom area were 1220 ± 310 mmol NO_3 m^{-2}, 68 ± 18 mmol PO_4 m^{-2} and 2360 ± 630 mmol $Si(OH)_4$ m^{-2} (Table 2), resulting in Si $(OH)_4$:NO_3 deficit ratios of 2.0 ± 0.4 mmol $mmol^{-1}$ and NO_3:PO_4 deficit ratios of 17 ± 1 mmol $mmol^{-1}$ in this region (Table 2, Fig. 3). 100 m averaged TDFe concentrations in this area were 0.14 ± 0.03 nM (Table 2, Fig. 4).

Due to the high variability within each bloom, no significant differences in nutrient concentrations or deficits were detected between the two study areas (Table 2). The ratios of $Si(OH)_4$:NO_3 deficits, however, were significantly lower in the 39 °W area compared to the 12 °W bloom (*t*-test, t=6.6, $p < 0.001$, n=35+26; Table 2, Fig. 3), while the ratios of NO_3:PO_4 deficits were significantly higher at 39 °W (*t*-test, t=15.4, $p < 0.001$, n=35+26).

4. Discussion

4.1. High variability of primary productivity in the APFZ

Two large-scale diatom-dominated phytoplankton blooms in the Atlantic sector of the ACC were observed (Fig. 1), both being located between 50 °S and 52 °S in the Antarctic Polar Frontal Zone (APFZ). Phytoplankton blooms are regularly observed in this region during spring and summer (e.g. Laubscher et al., 1993; Bathmann et al., 1997; Bracher et al., 1999; Tremblay et al., 2002). The occurrence of blooms in SO frontal zones has been associated with oceanographic frontal features such as jet streams, meanders and mesoscale eddies, which can lead to increased iron and silicate supply by mesoscale upwelling but also enhanced stratification due to cross-frontal overlayering (de Jong et al., 1998; Bracher et al., 1999; Strass et al., 2002a; Tremblay et al., 2002), thereby alleviating nutrient and light limitation for phytoplankton growth. In the Georgia Basin, bloom initialisation is thought to be mainly driven by iron input from South Georgia, while further east more complex modes of iron supply generate a larger degree of spatial and temporal variability in productivity (Venables and Meredith, 2009).

Being a relatively productive area within the otherwise HNLC (high-nutrient low-chlorophyll) region, the APFZ has been the destination of several research cruises (e.g. Bracher et al., 1999; Strass et al., 2002c; Tremblay et al., 2002; Korb and Whitehouse,

2004). Estimates of primary productivity in the APFZ vary between 100 and 6000 mg C m^{-2} d^{-1} (Mitchell and Holm-Hansen, 1991; Bracher et al., 1999; Moore and Abbott, 2000; Strass et al., 2002b; Tremblay et al., 2002; Hiscock et al., 2003; Vaillancourt et al., 2003; Korb and Whitehouse, 2004; Park et al., 2010), with the highest values being observed in the vicinity of land masses. The values observed in the present study are highly variable (about 160–3020 mg C m^{-2} d^{-1}; Table 1), but fall within the previously reported range. Antarctic phytoplankton productivity in this region has been reported to exhibit strong spatial (Veth et al., 1992; Arrigo et al. 1998), seasonal (Smith et al., 2000; Hiscock et al., 2003) and inter-annual variations (Clarke and Leakey, 1996; Park et al., 2010). Sporadic and patchy sampling during research cruises makes it therefore difficult to estimate the specific productivity in this region. These sampling opportunities are nonetheless useful to investigate the variability of productivity.

During sampling in the 12 °W bloom, one station in the initial centre of the bloom was investigated over a two-week period (Fig. 1, Table 1). Primary productivity estimates at this central sampling station varied between 1050 and 2820 mg C m^{-2} d^{-1} (Table 1). These values are in the same range as reported by Jochem et al. (1995), but considerably higher than previous estimates for this region (Bracher et al., 1999; Strass et al., 2002b; Tremblay et al., 2002; Korb and Whitehouse, 2004). The observed temporal variability, which was somewhat lower than the spatial variability in the 12 °W region (800–2820 mg C m^{-2} d^{-1}, Table 1), probably reflects a combination of the changes in light availability due to cloud cover (between 5 and 20 mol photons m^{-2} d^{-1}; Table 1) as well as the movement of water masses (Strass et al., 2017). The developmental phase of the phytoplankton bloom was also an important factor as primary production decreased over time (Table 1). During the investigation of the 39 °W bloom, emphasis was put on the spatial variability in productivity (Fig. 1, Table 1). In this bloom, primary productivity varied slightly more compared to the first area (570–3020 mg C m^{-2} d^{-1}; Table 1). This may be due to the higher spatial coverage, but also temporal aspects and the more dynamic currents play a role in this area (Strass et al., 2017). Nonetheless, even at three consecutive stations sampled on the same day (PS79/168-70) and within half a degree distance to each other, primary productivity varied between 790 and 2220 mg C m^{-2} d^{-1} (Table 1), demonstrating significant small-scale variability in the 39 °W bloom area (Leach et al., 2017).

The high spatial and temporal variability emphasises once more the difficulties in estimating the productivity in this highly dynamic region (Abbott et al., 2000). Even though satellite Chl *a* estimates have drawbacks compared to in-situ measurements (Schlitzer, 2002; Korb and Whitehouse, 2004; Whitehouse et al., 2008), they provide higher spatial and temporal coverage of phytoplankton biomass at mesoscale resolution. The satellite Chl *a* from the MERIS Polymer-Chl-product used in this study has been validated globally and regionally within the current *ESA Climate Change Initiative for Ocean colour* and was chosen as the best algorithm for MERIS data processing (Müller et al., 2015). Also in the current study, the quality of the satellite Chl *a* data (r^2=0.67, bias=0.17 mg m^{-3} compared to in-situ measurements) is sufficient to analyse the development of the two phytoplankton blooms at the surface. As satellite Chl *a* data only cover the ocean's first optical depth, estimates on primary productivity can only be derived using a model that incorporates satellite-based estimates of Chl *a*, sea surface temperature and PAR to reconstruct productivity over the entire mixed layer (e.g. Antoine and Morel, 1996). Shipboard Chl *a* and primary productivity data are therefore necessary in order to verify the accuracy of satellite-derived products and to give information on the layers below the first optical depth. ^{14}C-based estimates tend to overestimate primary productivity due to the exclusion of loss terms such as sinking or grazing as well as biases in applied irradiances (e.g. Gall et al., 2001). Nonetheless, this method can be used to investigate the underlying mechanisms for the patterns observed in satellite-derived maps.

4.2. Patterns in primary productivity do not correlate with MLDs

In the following, the two blooms are compared based on their general characteristics rather than investigating differences between single stations because relationships with the environmental conditions have to be considered on a wider scale, especially in such a highly dynamic region as the ACC.

In terms of depth-integrated primary productivity, no significant differences between the two blooms were observed during our visit (1750 ± 750 versus 1370 ± 830 mg C m^{-2} d^{-1}, *t*-test: $t=1.0$, $p=0.315$; Tables 1 and 2). Similar rates of primary productivity were achieved even though MLDs were significantly deeper in the 12 °W compared to the 39 °W bloom (71 ± 14 versus 35 ± 13 m, *t*-test: $t=6.0$, $p<0.001$; Table 2). Hence, despite spending different proportions of the day in the deep low-light environment, phytoplankton communities of both blooms established similar primary productivity (Fig. 5A; linear regression: $r^2=0.208$, $p=0.05$). This finding is somewhat surprising, as earlier studies suggested that the alleviation from light limitation through shoaling MLDs is a key determinant of bloom development and productivity in the open SO (Sambrotto and Mace, 2000; van Oijen et al., 2004; de Baar et al., 2005). In the current study, depth-integrated Chl *a* concentrations were positively correlated with MLD over the entire study area (Fig. 5B). POC:Chl *a* ratios were similar in both blooms (Table 2), indicating that Chl *a* as well as biomass build-up was not light limited in MLDs up to 90 m (Fig. 5A; linear regression: r^2 0.568, $p=0.0002$). In fact, depth-integrated primary productivity was best correlated with depth-integrated Chl *a* concentrations (Fig. 5C; linear regression: $r^2=0.718$, $p<0.0001$). Hence, phytoplankton cells were overall able to acclimate to different light regimes and sustained similar depth-integrated primary productivity at different MLDs.

It should be kept in mind, however, that the controlling role of light may be particularly important early in the growing season when deep surface mixing occurs, light availability is limited, and phytoplankton biomass is low (Bracher et al., 1999; Franck et al., 2000; Smith et al., 2000; Landry et al., 2002; Llort et al., 2015). The effects of light might explain the earlier onset of the 39 °W bloom (e.g. by stratification of the upper mixed layer), while the constant iron supply from South Georgia could have caused its longer duration. The light regime at the beginning of the growing season therefore may play an important role in modulating bloom dynamics by changing the rate and duration of biomass accumulation during the build-up phase of the bloom. Even though primary productivity did not differ between blooms, the depth-integrated photosynthetic efficiencies derived from Chl *a*-specific carbon fixation ($NPP_{Chl\ a}$) were higher in the 39 °W bloom compared to the 12 °W bloom area (*t*-test, $t=2.5$, $p=0.027$). In the more deeply mixed 12 °W bloom stations, lower $NPP_{Chl\ a}$-values indicate that phytoplankton photosynthesis was less efficient (Behrenfeld et al., 2008), possibly due to a combination of lower iron availability and deeper mixing regimes. Integrated over the water column, however, this did not lead to lower productivity than in the 39 °W bloom.

4.3. Nutrient deficits indicate differences in iron availability over the growing season

During the growing season, phytoplankton take up and export nutrients to a certain degree as part of particulate organic matter, which can be expressed as nutrient deficits or depletions (Le Corre and Minas, 1983; Jennings et al., 1984; Table 2). These proxies for net community production as well as their ratios differed between the two bloom areas (Fig. 3). While the ratios of $Si(OH)_4$:NO_3

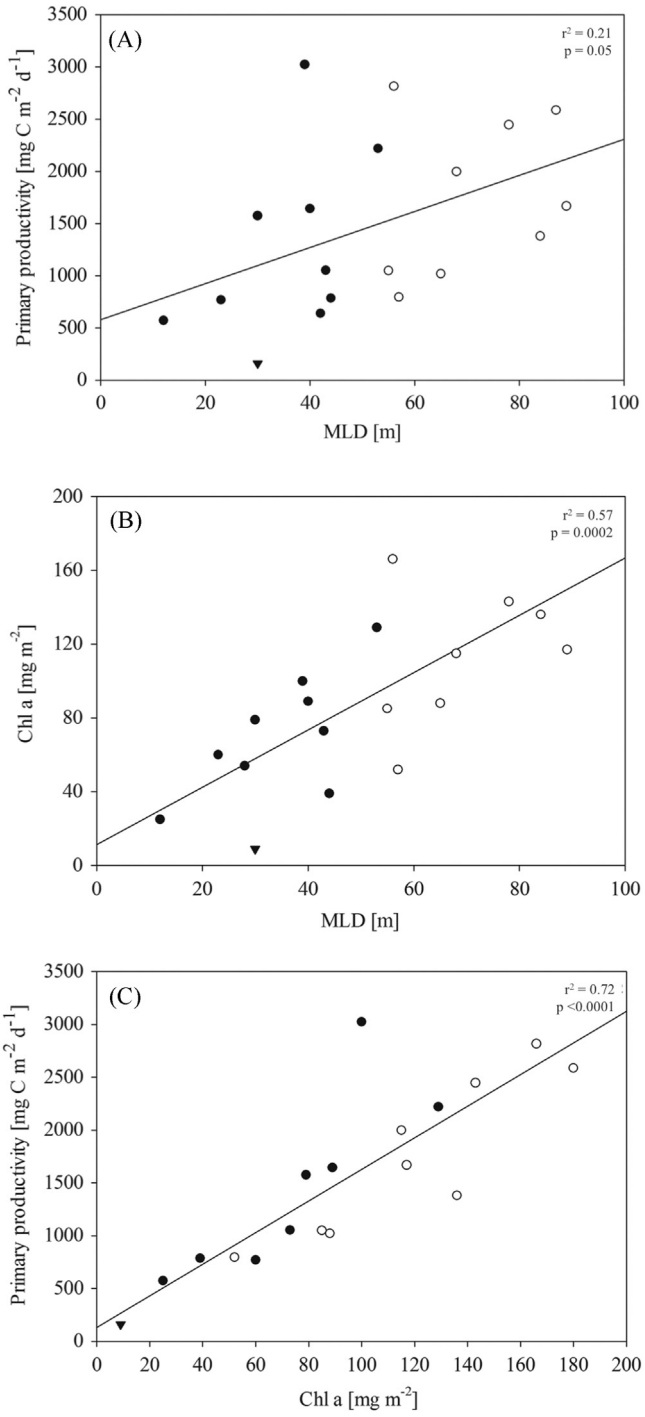

Fig. 5. Relationships between net primary production, mixed layer depth and Chl *a* – Depth-integrated NPP versus MLD (A), Chl *a* concentrations versus MLD (B) and NPP versus Chl *a* concentrations (C) for all stations in the 12 °W bloom (open circles) and the 39 °W bloom (filled circles) as well as the outstation (triangle). Lines indicate linear regression of all data.

deficits were significantly higher in the 12 °W compared to the 39 °W bloom area (*t*-test, $t=6.6$, $p<0.001$), the opposite trend was observed with respect to the NO_3:PO_4 deficit ratios (*t*-test: $t=15.4$, $p<0.001$). As phytoplankton need iron for the assimilation of nitrate (and to a lesser degree of phosphate), the absence of iron leads to lowered uptake capacities (de Baar et al., 1997; Hutchins and Bruland, 1998). While more generally, also taxonomic differences (e.g. diatom vs. flagellate dominated phytoplankton assemblages) affect nutrient deficit ratios, no such differences were observed in this study. And while shallow nitrification has been shown to influence SO nitrate concentrations in winter, it does not seem to influence nutrient concentrations and deficits in summer (Smart et al., 2015, cf. nitrate profiles in Fig. 2). Our results therefore indicate differences in the nutrient assimilation histories of the two diatom-dominated phytoplankton assemblages, which is likely due to differences in magnitude and dynamics of iron supply in the two regions (i.e. higher iron input in the 39 °W bloom area).

Drifter buoy trajectories indicate that water masses in the 39 °W sampling region, which originate from the South Georgia shelf (Meredith et al., 2003) and most likely receives a higher and steadier supply of iron and other trace metals (Korb and Whitehouse, 2004; Nielsdóttir et al., 2012; Borrione and Schlitzer, 2013; Strass et al., 2017). In the area around 12 °W, however, trace metal supply is thought to be restricted to deep-mixing during winter (Venables and Meredith, 2009), even though lateral transport could also play a role. During the time of sampling, iron measurements in the upper 100 m of the water column yielded similarly low dissolved (0.1–0.2 μmol m^{-3}; Fig. 5) and leachable particulate iron concentrations (0.2–0.8 μmol m^{-3}) in both areas (Table 2; Laglera et al., 2013, Laglera, unpubl. results), indicating iron depletion in both blooms. Given the development and intensity of the blooms as inferred from satellite data, iron concentrations must have been much higher at the onset of the blooms, yet they were already depleted by phytoplankton activity and particle scavenging at the time of sampling. Despite potentially large differences in iron availability and supply, surface silicate concentrations were similarly low in both areas and could potentially limit diatom growth (Fig. 2; Nelson et al., 2001). Furthermore, nutrient deficits were also similar even though phytoplankton accumulation started earlier in the 39 °W area (this study; Borrione and Schlitzer, 2013). These similarities of the two blooms can partly be explained by the lower $Si(OH)_4$:NO_3 assimilation ratios at 39 °W (Table 2), but may also suggest differences in the intensity of nutrient cycling, export and grazing pressure between the two systems.

4.4. From bottom-up towards top-down controls

Nutrient deficits can be used to estimate season-integrated net community production and are thus a proxy for new production on an annual basis (Jennings et al., 1984; Strass and Woods, 1991; Hoppema et al., 2000; Whitehouse et al., 2012). Production rates calculated from nutrient deficits, however, can potentially be biased by altered nutrient concentrations due to vertical or lateral mixing and advection, alternative nutrient sources (e.g. ammonium), as well as changes in stoichiometry of organic matter (Jennings et al., 1984; Hoppema et al., 2007; Whitehouse et al., 2012). In agreement with Laubscher et al. (1993), slightly stronger nutrient depletion in the 39 °W region co-occurred with higher photosynthetic efficiencies compared to 12 °W (Table 2). This could indicate a better acclimation to their environment in the former bloom, potentially resulting from higher and steadier iron supply as well as easier photoacclimation in shallower mixed layers. The estimates of primary productivity and POC:PON as well as POC:Chl *a* ratios (Tables 1 and 2), however, were in a similar range for both blooms. Furthermore, nutrient deficits, though somewhat lower in the 12 °W bloom region, were not remarkably different between regions (Fig. 3, Table 2). This is surprising, particularly in view of the almost two months earlier onset of the bloom in the Georgia Basin.

This apparent contradiction could have been caused by lower export efficiencies in the 39 °W bloom. Shipboard carbonate chemistry measurements, however, revealed higher deficits in dissolved inorganic carbon (DIC) and a stronger CO_2 uptake from

the atmosphere in the 39 °W compared to the 12 °W bloom area (Jones et al., 2017). Therefore, the mismatch between nutrient deficits and bloom dynamics (as observed via satellites) was more likely caused by the highly dynamic currents in the 39 °W area (Strass et al., 2017), which may have led to an underestimation of seasonal nutrient deficits due to higher lateral nutrient input (Oschlies, 2002). Furthermore, net productivity may have been overestimated to different degrees in both blooms because loss terms such as grazing tend to be underestimated in ^{14}C-based measurements (e.g. Gall et al., 2001).

Recent field-, satellite- and model-based studies have highlighted the thus-far underestimated importance of top-down control mechanisms for phytoplankton bloom dynamics (e.g. Behrenfeld and Boss, 2014; Llort et al., 2015). As the average zooplankton biomass in the South Georgia area is larger than anywhere else in the Southern Ocean (Atkinson et al., 2001), we speculate that during the time of sampling, top-down control was more strongly developed in the 39 °W compared to the 12 °W bloom area. Zooplankton sampling during our cruise showed that, despite high spatial variability, the zooplankton community around 39 °W was in a more progressed state of development compared to the 12 °W bloom area. In the latter, the proportion of small organisms and early developmental stages was higher (Pakomov and Hunt, unpubl. data). A potentially lower grazing pressure in the 12 °W bloom could also be explained by a lower probability for predator–prey encounters in deeper MLDs (Behrenfeld, 2010). In fact, this dilution effect on grazing rates might have contributed to the positive correlation between biomass and MLD found throughout our study (Fig. 5B).

As the control of phytoplankton bloom dynamics in the ACC can shift from bottom-up to mainly top-down within a few weeks (Abbott et al., 2000; Llort et al., 2015), also a slightly earlier bloom development at 39 °W could have led to our observations. Diatom-dominated blooms, as observed in this study (Klaas, unpubl. results), are mainly grazed by larger zooplankton. One can therefore assume that the usual time lag between bloom and grazer development (Smetacek et al. 2004) was still allowing phytoplankton biomass build-up in the 12 °W area, while grazers already imposed a strong control on the 39 °W bloom during the time of sampling. Satellite Chl *a* maps of the two bloom areas indeed show that the 39 °W bloom developed around 8 weeks earlier than the 12 °W bloom. We thus conclude that, despite both being in the apex phase, we visited the two areas at different stages of the bloom development.

5. Conclusions and biogeochemical implications

The results of this study suggest that a combination of different drivers strongly affect primary productivity in the SO. Bottom-up processes control the rate of build-up of a bloom, while top-down processes seem to be more important for determining the phytoplankton standing stock at the late bloom stage, i.e. when sampling took place (Fig. 6). In contrast to earlier suggestions (van Oijen et al., 2004; de Baar et al., 2005), we did not observe significant light limitation of phytoplankton communities in two highly productive open-ocean areas of the Atlantic sector of the SO. Our results indeed indicate that, despite MLDs being deeper than 90 m, this does not necessarily prevent the development of phytoplankton blooms in the APFZ. Instead, iron supply seems to be the bottom-up process playing a pivotal role, particularly for determining bloom development and its potential duration, but also by modulating the light-use efficiency of phytoplankton (Smetacek et al., 2012; Behrenfeld and Milligan, 2013). Considering the time scales of the individual measurements, we were thus able to explain the observed patterns by differences in iron availability and grazing pressure.

Acknowledgments

We would like to thank all scientists as well as the captain, officers and crew of RV Polarstern for their work and support during the ANT-XXVIII/3 cruise. Especially, we would like to thank E. Jones and M. Iversen for helpful discussions on the present dataset. We thank S. Wiegmann for help with the HPLC analysis, F. Steinmetz (HYGEOS) for supplying Polymer-MERIS CHL data and ESA for MERIS level-1 satellite data. We also thank E. Jones for providing DIC

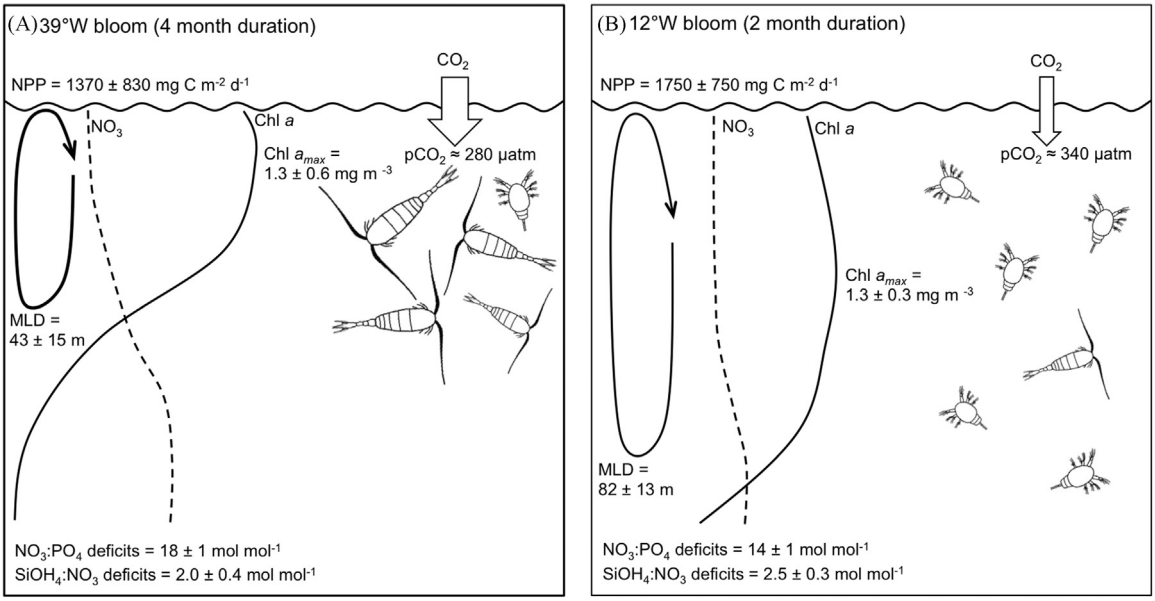

Fig. 6. Schematic overview – Similarities of and differences between the 39 °W (A) and the 12 °W bloom (B) in terms of MLDs, nutrient concentrations and deficits, NPP and pCO_2 as well as Chl *a* and zooplankton standing stocks.

measurements. Furthermore, we would like to thank F. Altvater, D. Kottmeier, R. Kottmeier, T. Rueger, V. Schourup-Kristensen for their help during the cruise as well as A. Terbrüggen, K.-U. Richter and U. Richter for help with the cruise preparations. C.J.M.H. and B.R. were funded by the European Research Council (ERC) under the European Community's Seventh Framework Programme (FP7/2007-2013), ERC Grant agreement no. 205150. S.T. was funded by the German Science Foundation (DFG), project TR 899/2 and the Helmholtz Impulse Fond (HGF Young Investigator Group EcoTrace). Funding to M.S. was supplied by CAPES, Brazil (Grant BEX 3483/09-6), and to A.B. by the Helmholtz Innovation Fund Phytooptics. This work was funded by the MINECO of Spain (Grant CGL2010-11846-E) and the Government of the Balearic Islands (Grant AAEE083/09). J.S.E. was supported by the JAE-Doc program of the CSIC. M.H. was supported through EU FP7 project CARBOCHANGE, which received funding from the European Community's Seventh Framework Programme under Grant agreement no. 264879. This work was furthermore supported by the DFG in the framework of the priority programme "Antarctic Research with comparative investigations in Arctic ice areas" by a Grant HO 4680/1.

References

Abbott, M.R., Richman, J.G., Letelier, R.M., Bartlett, J.S., 2000. The spring bloom in the Antarctic polar frontal zone as observed from a mesoscale array of bio-optical sensors. Deep-Sea Res. Part II: Top. Stud. Oceanogr. 47, 3285–3314.

Antoine, D., Morel, A., 1996. Oceanic primary production: I. Adaptation of a spectral light-photosynthesis model in view of application to satellite chlorophyll observations. Glob. Biogeochem. Cycles 10, 43–55.

Arrigo, K.R., Worthen, D., Schnell, A., Lizotte, M.P., 1998. Primary production in Southern Ocean waters. J. Geophys. Res.: Oceans 103, 15587–15600.

Atkinson, A., Whitehouse, M.J., Priddle, J., Cripps, G.C., Ward, P., Brandon, M.A., 2001. South Georgia, Antarctica: a productive, cold water, pelagic ecosystem. Mar. Ecol. Prog. Ser. 216, 279–308.

Bathmann, U.V., Scharek, R., Klaas, C., Dubischar, C.D., Smetacek, V., 1997. Spring development of phytoplankton biomass and composition in major water masses of the Atlantic sector of the Southern Ocean. Deep-Sea Res. Part II: Top. Stud. Oceanogr. 44, 51–67.

Behrenfeld, M.J., 2010. Abandoning Sverdrup's critical depth hypothesis on phytoplankton blooms. Ecology 91, 977–989.

Behrenfeld, M.J., Halsey, K.H., Milligan, A.J., 2008. Evolved physiological responses of phytoplankton to their integrated growth environment. Philos. Trans. R. Soc. B: Biol. Sci. 363, 2687–2703.

Behrenfeld, M.J., Milligan, A.J., 2013. Photophysiological expressions of iron stress in phytoplankton. Annu. Rev. Mar. Sci. 5, 217–246.

Behrenfeld, M.J., Boss, E.S., 2014. Resurrecting the ecological underpinnings of ocean plankton blooms. Annu. Rev. Mar. Sci. 6, 167–194.

Blain, S., Tréguer, P., Belviso, S., Bucciarelli, E., et al., 2001. A biogeochemical study of the island mass effect in the context of the iron hypothesis: Kerguelen islands, Southern Ocean. Deep-Sea Res. Part I: Oceanogr. Res. Pap. 48, 163–187.

Borrione, I., Schlitzer, R., 2013. Distribution and recurrence of phytoplankton blooms around South Georgia, Southern Ocean. Biogeosciences 10, 217–231.

Bracher, A.U., Kroon, B.M.A., Lucas, M.I., 1999. Primary production, physiological state and composition of phytoplankton in the Atlantic sector of the Southern Ocean. Mar. Ecol. Prog. Ser. 190, 1–16.

Brzezinski, M.A., Dickson, M.-L., Nelson, D.M., Sambrotto, R., 2003. Ratios of Si, C and C uptake by microplankton in the Southern Ocean. Deep-Sea Res. Part II: Top. Stud. Oceanogr. 50, 619–633.

Cheah, W., et al., 2017. Importance of silicic acid in regulating phytoplankton biomass and community structure in the iron-limited Antarctic Polar Front, Deep. Sea Res. Part II: Top. Stud. Oceanogr. 138, 74–85.

Cisewski, B., Strass, V.H., Prandke, H., 2005. Upper-ocean vertical mixing in the Antarctic Polar Front Zone. Deep. Sea Res. Part II: Top. Stud. Oceanogr. 52, 1087–1108.

Clarke, A., Leakey, R.J., 1996. The seasonal cycle of phytoplankton, macronutrients, and the microbial community in a nearshore antarctic marine ecosystem. Limnol. Oceanogr. 41, 1281–1294.

de Baar, H., Boyd, P., Coale, K., Landry, M., Tsuda, A., et al., 2005. Synthesis of iron fertilization experiments: from the iron age in the age of enlightenment. J. Geophys. Res. Oceanogr. 110, C09S16.

de Baar, H.J.W., de Jong, J.T.M., Bakker, D.C.E., Loscher, B.M., Veth, C., Bathmann, U., Smetacek V, V., 1995. Importance of iron for plankton blooms and carbon dioxide drawdown in the Southern Ocean. Nature 373, 412–415.

de Baar, H.J.W., Van Leeuwe, M.A., Scharek, R., Goeyens, L., Bakker, K.M.J., Fritsche, P., 1997. Nutrient anomalies in *Fragilariopsis kerguelensis* blooms, iron deficiency and the nitrate/phosphate ratio (A.C. Redfield) of the Antarctic Ocean. Deep-Sea Res. Part II: Top. Stud. Ocean. 44, 229–260.

de Jong, J.T.M., den Das, J., Bathmann, U., MHC, Stoll, Kattner, G., Nolting, R.F., HJW, de Baar, 1998. Dissolved iron at subnanomolar levels in the Southern Ocean as determined by ship-board analysis. Anal. Chim. Acta 377, 113–124.

Dubischar, C.D., Bathmann, U.V., 1997. Grazing impact of copepods and salps on phytoplankton in the Atlantic sector of the Southern Ocean. Deep-Sea Res. Part II: Top. Stud. Oceanogr. 44, 415–433.

Dugdale, R.C., Goering, J.J., 1967. Uptake of new and regenerated forms of nitrogen in primary productivity. Limnol. Oceanogr. 12, 196–206.

Eppley, R.W., Peterson, B.J., 1979. Particulate organic matter flux and planktonic new production in the deep ocean. Nature 282, 677–680.

Falkowski, P.G., Barber, R.T., Smetacek, V., 1998. Biogeochemical controls and feedbacks on ocean primary production. Science 281, 200–206.

Field, C.B., Behrenfeld, M.J., Randerson, J.T., Falkowski, P., 1998. Primary production of the biosphere: integrating terrestrial and oceanic components. Science 281, 237–240.

Franck, V.M., Brzezinski, M.A., Coale, K.H., Nelson, D.M., 2000. Iron and silicic acid concentrations regulate Si uptake north and south of the Polar Frontal Zone in the Pacific Sector of the Southern Ocean. Deep Sea Research Part II: Topical Studies in Oceanography 47, 3315–3338.

Gall, M.P., Strzepek, R., Maldonado, M., Boyd, P.W., 2001. Phytoplankton processes. Part 2: rates of primary production and factors controlling algal growth during the Southern Ocean iron release experiment (SOIREE). Deep-Sea Res. Part II: Top. Stud. Ocean. 48, 2571–2590.

Grasshoff, K., Kremling, K., Ehrhardt, M., 1999. Methods of Seawater Analysis. Wiley-VCH, Weinheim.

Hiscock, M.R., Marra, J., Smith, W.O., Goericke, R., et al., 2003. Primary productivity and its regulation in the Pacific sector of the Southern Ocean. Deep-Sea Res. II 50, 533–558.

Hoffmann, L.J., Peeken, I., Lochte, K., Assmy, P., Veldhuis, M., 2006. Different reactions of Southern Ocean phytoplankton size classes to iron fertilization. Limnol. Oceanogr. 51, 1217–1229.

Hoppema, M., Goeyens, L., Fahrbach, E., 2000. Intense nutrient removal in the remote area off Larsen Ice Shelf (Weddell Sea). Polar Biol. 23, 85–94.

Hoppema, M., Middag, R., de Baar, H.J.W., Fahrbach, E., van Weerlee, E.M., Thomas, H., 2007. Whole season net community production in the Weddell Sea. Polar Biol. 31, 101–111.

Hutchins, D., Bruland, K., 1998. Iron-limited diatom growth and Si:N uptake ratios in a coastal upwelling regime. Nature 393, 561.

Jennings, J.C., Gordon, L.I., Nelson, D.M., 1984. Nutrient depletion indicates high primary productivity in the Weddell Sea. Nature 309, 51–54.

Jochem, F., Mathot, S., Quéguiner, B., 1995. Size-fractionated primary production in the open Southern Ocean in Austral Spring. Polar Biol. 15, 381–392.

Jones, E.M., Hoppema, M., Strass, V., Hauck, J., Salt, L., Klaas, C., van Heuven S.M.A.C., Wolf-Gladrow D., de Baar H.J.W., 2017. Mesoscale features create hotspots of carbon uptake in the Antarctic Circumpolar Current, Deep. Sea Res. Part II: Top. Stud. Oceanogr. 138, 39–51.

Knap, A., Michaels, A., Close, H.D., Dickson, A, 1996. Protocols for the joint global ocean flux study (JGOFS) core measurements. UNESCO.

Korb, R.E., Whitehouse, M., 2004. Contrasting primary production regimes around South Georgia, Southern Ocean: large blooms versus high nutrient, low chlorophyll waters. Deep-Sea Res. Part I: Oceanogr. Res. Pap. 51, 721–738.

Laglera, L.M., Santos-Echeandía, J., Caprara, S., Monticelli, D., 2013. Quantification of iron in seawater at the low picomolar range based on optimization of bromate/ammonia/ dihydroxynaphtalene system by catalytic adsorptive cathodic stripping voltammetry. Anal. Chem. 85, 2486–2492.

Landry, M.R., Selph, K.E., Brown, S.L., Abbott, M.R., et al., 2002. Seasonal dynamics of phytoplankton in the Antarctic polar front region at 170 °W. Deep-Sea Res. Part II: Top. Stud. Oceanogr. 49, 1843–1865.

Leach, H., Strass, V., Prandke, H., 2017. Mixing and finescale structures in two mesoscale features of the Antarctic Circumpolar Current, Deep. Sea Res. Part II: Top. Stud. Oceanogr. 138,.

Laubscher, R.K., Perissinotto, R., McQuaid, C.D., 1993. Phytoplankton production and biomass at frontal zones in the Atlantic sector of the Southern Ocean. Polar Biol. 13, 471–481.

Le Corre, P., Minas, H.J., 1983. Distributions et évolution des éléments nutritifs dans le secteur indien de l'Océan Antarctique en fin de période estivale. Ocean. Acta 6, 365–381.

Llort, J., Lévy, M., Sallée, J.-B., Tagliabue, A., 2015. Onset, intensification, and decline of phytoplankton blooms in the Southern Ocean. ICES J. Mar. Sci.: J. Du. Cons. (in press)

Longhurst, A.R., Harrison, W.G., 1989. The biological pump: profiles of plankton production and consumption in the upper ocean. Prog. Oceanogr. 22, 47–123.

Lorrain, A., Savoye, N., Chauvaud, L., Paulet, Y.-M., Naulet, N., 2003. Decarbonation and preservation method for the analysis of organic C and N contents and stable isotope ratios of low-carbonated suspended particulate material. Anal. Chim. Acta 491, 125–133.

Martin, J.H., 1990. Glacial-interglacial CO_2 change: the iron hypothesis. Paleoceanography 5, 1–13.

Meredith, M.P., Watkins, J.L., Murphy, E.J., Cunningham, N.J., et al., 2003. An anticyclonic circulation above the northwest Georgia Rise, Southern Ocean. Geophys. Res. Lett. 30, GL018039.

Mitchell, B.G., Holm-Hansen, O., 1991. Observations and modeling of the Antarctic phytoplankton crop in relation to mixing depth. Deep-Sea Res. 38, 981–1007.

Moore, J.K., Abbott, M.R., 2000. Phytoplankton chlorophyll distributions and primary production in the southern ocean. J. Geophys. Res.: Ocean. 105, 28709–28722.

Moore, J.K., Abbott, M.R., Richman, J.G., Nelson, D.M., 2000. The Southern Ocean at the last glacial maximum: a strong sink for atmospheric carbon dioxide. Glob. Biogeochem. Cycles 14, 455–475.
Moore, J.K., Abbott, M.R., Richman, J.G., Smith, W.O., et al., 1999. SeaWiFs satellite ocean color data from the Southern Ocean. Geophys. Res. Lett. 26, 1465–1468.
Morel, A., Huot, Y., Gentili, B., Werdell, P.J., Hooker, S.B., Franz, B.A., 2007. Examining the consistency of products derived from various ocean color sensors in open ocean (case 1) waters in the perspective of a multi-sensor approach. Remote. Sens. Environ. 111, 69–88.
Müller, D., Krasemann, H., Brewin, R.J.W., Brockmann, C., Deschams, P.-Y., et al., 2015. The Ocean colour climate change initiative: II. Spatial and temporal homogeneity of satellite data retrieval due to systematic effects in atmospheric correction processors. Remote. Sens. Environ 162, 257–270.
Murphy, J., Riley, J.P., 1962. A modified single solution method for the determination of phosphate in natural waters. Anal. Chim. Acta 27, 31–36.
Nelson, D.M., Brzezinski, M.A., Sigmon, D.E., Franck, V.M., 2001. A seasonal progression of Si limitation in the pacific sector of the Southern Ocean. Deep-Sea Res. Part II: Top. Stud. Oceangr. 48, 3973–3995.
Nelson, D.M., Smith, W.O.J., 1991. Sverdrup revisited: critical depths, maximum chlorophyll levels, and the control of Southern Ocean productivity by the irradiance-mixing regime. Limnol. Oceanogr. 36, 1650–1661.
Nielsdóttir, M.C., Bibby, T.S., Moore, C.M., Hinz, D.J., Sanders, R., et al., 2012. Seasonal and spatial dynamics of iron availability in the Scotia Sea. Marine Chemistry 131, 62–72.
Oschlies, A., 2002. Nutrient supply to the surface waters of the North Atlantic: a model study. J. Geophys. Res.: Oceans 107, 14-1–14-13.
Park, J., Oh, I.-S., Kim, H.-C., Yoo, S., 2010. Variability of SeaWiFs Chlorophyll-a in the southwest Atlantic sector of the Southern Ocean: strong topographic effects and weak seasonality. Deep-Sea Res. Part I: Oceanogr. Res. Pap. 57, 604–620.
Petrou, K., Trimborn, S., Rost, B., Ralph, P., Hassler, C., 2014. The impact of iron limitation on the physiology of the Antarctic diatom Chaetoceros simplex. Mar. Biol., 1–13.
Priddle, J., Smetacek, V., Bathmann, U., Stromberg, J.-O., Croxall, J.P., 1992. Antarctic marine primary production, biogeochemical carbon cycles and climatic change. Philos. Trans. R. Soc. Lond. Ser. B: Biol. Sci. 338, 289–297.
Sambrotto, R.N., Mace, B.J., 2000. Coupling of biological and physical regimes across the Antarctic Polar Front as reflected by nitrogen production and recycling. Deep. Sea Res. Part II: Top. Stud. Oceanogr. 47, 3339–3367.
Schlitzer, R., 2002. Carbon export fluxes in the Southern Ocean: results from inverse modeling and comparison with satellite based estimates. Deep-Sea Res. II 49, 1623–1644.
Smart, S.M., Fawcett, S.E., Thomalla, S.J., Weigand, M.A., Reason, C.J.C., et al., 2015. Isotopic evidence for nitrification in the Antarctic winter mixed layer. Glob. Biogeochem. Cycles 29, 427–445.
Smetacek, V., Assmy, P., Henjes, J., 2004. The role of grazing in structuring Southern Ocean pelagic ecosystems and biogeochemical cycles. Antarct. Sci. 16, 541–558.
Smetacek, V., et al., 2012. Deep carbon export from a Southern Ocean iron-fertilized diatom bloom. Nature 487, 313–319.
Smith Jr, W.O., Marra, J., Hiscock, M.R., Barber, R.T., 2000. The seasonal cycle of phytoplankton biomass and primary productivity in the Ross Sea, Antarctica. Deep-Sea Res. Part II: Top. Stud. Ocean. 47, 3119–3140.
Steinmetz, F., Deschamps, P.Y., Ramon, D., 2011. Atmospheric correction in presence of sun glint: application to MERIS. Opt. Express 19, 9783–9800.
Strass, V.H., Woods, J.D., 1991. New production in the summer revealed by the meridional slope of the deep chlorophyll maximum. Deep-Sea Res. 38 (1), 35–56.
Strass, V.H., Naveira Garabato, A.C., Pollard, R.T., Fischer, H.I., et al., 2002a. Mesoscale frontal dynamics: shaping the environment of primary production in the Antarctic Circumpolar Current. Deep-Sea Res. Part II: Top. Stud. Oceanogr. 49, 3735–3769.
Strass, V.H., Naveira Garabato, A.C., Bracher, A.U., Pollard, R.T., Lucas, M.I., 2002b. A 3-D mesoscale map of primary production at the Antarctic Polar Front: results of a diagnostic model. Deep-Sea Res. Part II: Top. Stud. Oceanogr. 49, 3813.
Strass, V.H., Bathmann, U., Rutgers v. d. Loeff, M., Smetacek, V., 2002c. Mesoscale physics, biogeochemistry and ecology of the Antarctic Polar Front, Atlantic Sector: an introduction to and summary of cruise ANT-XIII/2 of RV Polarstern. Deep-Sea Res. II: Top. Stud. Oceanogr. 49, 3707–3711.
Strass, V.H., Leach, H., Prandke, H., Donnelly, M., Bracher, A.U., Wolf-Gladrow, D.A., 2017. The physical environmental conditions of biogeochemical differences along the ACC in the Atlantic Sector during late austral summer 2012, Deep. Sea Res. Part II: Top. Stud. Oceanogr. 138, 6–25.
Strickland, J.D.H., Parsons, T.R., 1968. A Practical Handbook of Seawater Analysis, Vol Bulletin. No. 167. Fisheries Research Board of Canada.
Sunda, W.G., Huntsman, S.A., 1997. Interrelated influence of iron, light and cell size on marine phytoplankton growth. Nature 390, 389–392.
Tremblay, J.E., Lucas, M.I., Kattner, G., Pollard, R., Bathmann, U., Strass, V., Bracher, A., 2002. Significance of the Polar Frontal Zone for large-sized diatoms and new production during summer in the Atlantic Sector of the Southern Ocean. Deep-Sea Res. II 49 (18), 3793–3811.
van Oijen, T., van Leeuwe, M.A., Granum, E., Weissing, F.J., Bellerby, R.G.J., et al., 2004. Light rather than iron controls photosynthate production and allocation in Southern Ocean phytoplankton populations during austral autumn. J. Plankton Res. 26, 885–900.
Vaillancourt, R.D., Marra, J., Barber, R.T., Smith Jr, W.O., 2003. Primary productivity and in situ quantum yields in the Ross Sea and pacific sector of the Antarctic Circumpolar Current. Deep-Sea Res. Part II: Top. Stud. Oceanogr. 50, 559–578.
Venables, H.J., Meredith, M.P., 2009. Theory and observations of Ekman flux in the chlorophyll distribution downstream of South Georgia. Geophys. Res. Lett. 36, GL23610.
Veth, C., Lancelot, C., Ober, S., 1992. On processes determining the vertical stability of surface waters in the marginal ice zone of the north-western Weddell Sea and their relationship with phytoplankton bloom development. Polar Biol. 12, 237–243.
Whitehouse, M.J., Atkinson, A., Korb, R.E., Venables, H.J., Pond, D.W., Gordon, M., 2012. Substantial primary production in the land-remote region of the central and northern Scotia Sea. Deep-Sea Res. Part II: Top. Stud. Oceanogr. 59–60, 47–56.
Whitehouse, M.J., Korb, R.E., Atkinson, A., Thorpe, S.E., Gordon, M., 2008. Formation, transport and decay of an intense phytoplankton bloom within the high-nutrient low-chlorophyll belt of the Southern Ocean. J. Mar. Syst. 70, 150–167.
Wolf-Gladrow, D., 2013. The expedition of the research vessel "Polarstern" to the Antarctic in 2012 (ANT-XXVIII/3). Berichte zur Polar- und Meeresforschung Reports on Polar and Marine Research. 661. Alfred Wegener Institute for Polar and Marine Research, Bremerhaven, p. 191.